

Linear and nonlinear optical spectroscopy of a strongly-coupled microdisk-quantum dot system

Kartik Srinivasan^{1,*} and Oskar Painter^{2,†}

¹Center for the Physics of Information, California Institute of Technology, Pasadena, CA

²Thomas J. Watson, Sr., Laboratory of Applied Physics,
California Institute of Technology, Pasadena, CA 91125

(Dated: October 30, 2018)

A fiber taper waveguide is used to perform direct optical spectroscopy of a microdisk-quantum-dot system, exciting the system through the *photonic* (light) channel rather than the *excitonic* (matter) channel. Strong coupling, the regime of coherent quantum interactions, is demonstrated through observation of vacuum Rabi splitting in the transmitted and reflected signals from the cavity. The fiber coupling method also allows the examination of the system's steady-state nonlinear properties, where saturation of the cavity-QD response is observed for less than one intracavity photon.

Cavity quantum electrodynamics¹, the study of coherent quantum interactions between the electromagnetic field and matter inside a resonator, has received attention as both a testbed for ideas in quantum mechanics and also as a building block for applications in the field of quantum information processing². The canonical experimental system studied in the optical domain is a single alkali atom coupled to a high-finesse Fabry-Perot cavity. The tremendous progress made in this system^{1,2,3,4,5} has been complemented by recent research involving trapped ions⁶, chip-based microtoroid cavities⁷, integrated microcavity-atom-chips⁸, nanocrystalline quantum dots coupled to microsphere cavities⁹, and semiconductor quantum dots embedded in micropillars, photonic crystals, and microdisks^{10,11,12}. The latter system has been of particular interest due to its potential simplicity and scalability. In contrast to preceding work with semiconductor systems, which has focused on photoluminescence measurements^{10,11,12,13,14}, here we use a fiber taper waveguide to perform direct optical spectroscopy of a microdisk-quantum-dot system, exciting the system through the *photonic* (light) channel rather than the *excitonic* (matter) channel. Strong coupling, the regime of coherent quantum interactions, is demonstrated through observation of vacuum Rabi splitting in the transmitted and reflected signals from the cavity. The fiber coupling method also allows us to examine the system's steady-state nonlinear properties, where we see a saturation of the cavity-QD response for less than one intracavity photon. The excitation of the cavity-QD system through a fiber optic waveguide is key for applications such as high-efficiency single photon sources^{15,16}, and to more fundamental studies of the quantum character of the system¹⁷.

In the most simplified picture, cavity quantum electrodynamics (cQED) consists of a single two-level atom (or equivalent) coupled to an electromagnetic mode of a cavity. A more realistic picture includes dissipative processes, such as cavity loss and atomic decoherence, and excitation of the system, either through the atomic or photonic channel. The observed system response is dependent on both which channel is excited, and what signal is measured. Previous demonstrations of strong coupling between semiconductor microcavities

and quantum dots (QDs)^{10,11,12,13,14} used non-resonant optical pumping to excite the QD stochastically and photoluminescence (PL) to probe the system behavior. In this work we excite the system coherently through the photonic channel, and detect signatures of cavity-QD coupling in the resonant optical response. Such optical spectroscopy is commonplace in atom-Fabry-Perot systems¹, but is more problematic in semiconductor microcavities due to the comparative difficulty in effectively coupling light into and out of sub-micron structures. To effectively interface with the cavity, we use an optical fiber taper waveguide¹⁸. Fiber tapers are standard glass optical fibers that have been heated and stretched to a diameter at or below the wavelength of light, at which point the evanescent field of the guided mode extends into the surrounding air and allows the taper to function as a near-field optic^{7,19,20,21}.

The experimental setup used is shown schematically in Fig. 1(a)-(b). At its core is a customized liquid He cryostat²² in which piezo-actuated stages have been integrated to incorporate optical fiber taper testing while maintaining a sample temperature as low as 12 K. External cavity tunable lasers optically pump the QD and probe the cavity-QD system near-resonance, and fused-fiber couplers direct the cavity's reflected and transmitted signals to photodetectors and a spectrometer. The overall transmission of the fiber taper link is 50% in this work, and in many cases can be $\gtrsim 90\%$, providing a very low-loss optical channel to probe the system. This allows for the accurate estimation of quantities such as average intra-cavity photon number through measurement of the resonant transmission of the taper waveguide when coupled to the cavity.

The system under investigation consists of InAs QDs embedded in a GaAs microdisk cavity. The InAs QDs are grown in a self-assembled manner with a density of $300 - 500 \mu\text{m}^{-2}$ on top of an InGaAs quantum well (a so-called dot-in-a-well, or DWELL²³). The DWELL structure resides in the middle of a 256 nm thick GaAs layer that forms the thin planar layer of the microdisk (see Fig. 1(c)). Previous studies of this material²⁴ indicate that isolated emission from single QDs at cryogenic temperature can be seen in the wavelength range $\lambda = 1290\text{-}1310$ nm, approximately 50 nm red-shifted from the peak of the QD ensemble emission. Microdisks of diameter $D = 2.5 \mu\text{m}$ are created through electron beam lithography, plasma dry etching, and wet undercut etching²¹. Finite-element-method (FEM) simulations (Fig. 1(d-e)) of

*Electronic address: kartik@caltech.edu

†Electronic address: opainter@caltech.edu

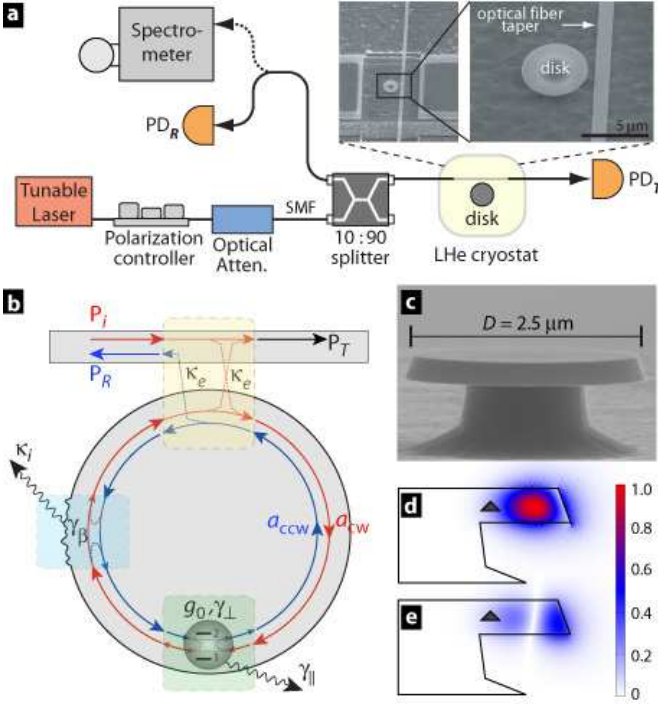


FIG. 1: Schematics of the experimental apparatus and system. **a**, Diagram of the experimental setup showing a scanning electron microscope (SEM) image of a taper-coupled microdisk. $PD_{R/T}$ are photodetectors for the reflected/transmitted signals. **b**, Illustration of the coupled microdisk-QD system. $a_{CW/CCW}$ are the amplitudes for the clockwise/counterclockwise modes, $P_{i/R/T}$ are the incident/reflected/transmitted signals, and κ_e and κ_i correspond to the fiber-to-cavity coupling and intrinsic cavity field decay rates, respectively. **c**, SEM image of one of the small microdisk cavities under study. **d**, FEM simulations of the radial (E_ρ) and **e**, azimuthal (E_ϕ) electric field components of the $TE_{p=1, m=13}$ mode in cross-section. p denotes the radial order and m the azimuthal mode number. The shaded triangle indicates the estimated QD position in this work.

the microdisks show that the $TE_{1,13}$ whispering gallery mode (WGM) is resonant at $\lambda \sim 1300$ nm. This optical mode has a radiation-limited quality factor $Q_{\text{rad}} > 10^8$, and an effective standing wave mode volume $V_{\text{sw}} = 3.2(\lambda/n)^3$. The peak coherent coupling rate for a QD excitonic state of the type studied here (i.e., spontaneous emission lifetime $\tau_{\text{sp}} = 1$ ns) with optimal placement and dipole orientation is $g_0/2\pi = 15$ GHz. Since our QDs are not deterministically positioned in the cavity as in recent studies²⁵, the actual exhibited coupling rate g may be significantly smaller (see Methods). The magnitude of g relative to the system decay rates, κ_T (cavity field decay) and γ_\perp (QD dephasing), determines whether the system lies in the perturbative (weak coupling: $g < (\kappa_T, \gamma_\perp)$) or non-perturbative (strong coupling: $g > (\kappa_T, \gamma_\perp)$) regime of cQED¹.

The process by which we identify a suitable device for studying cavity-QD coupling is described in the Methods section. Figure 2(a) shows the fiber-taper-collected PL spectrum from one such device that has been cooled down to 15 K. Optical pumping of the QD is provided by exciting (also through

the taper) a blue-detuned higher-order WGM of the disk at $\lambda_P \sim 982.2$ nm. The cavity mode, which is fed by background emission processes¹³, is the tall peak at the blue end of the spectrum. The three emission peaks red of the cavity mode are the fine-structure-split²⁶ neutral single exciton lines, X_a and X_b , and the negatively charged single exciton line, X^- .

Further insight into the coupled cavity-QD system from PL are masked by the limited resolution of our spectrometer (35 pm). In this case the interesting behavior of the cavity-QD coupling can be studied by resonant spectroscopy of the cavity mode using a fiber-coupled, narrowband (linewidth < 5 MHz) tunable laser. The inset to Fig. 2(a) shows the taper's transmission spectrum when it is placed in contact with the side of the microdisk cavity and the cavity modes are detuned from the exciton lines. As has been described in previous work²¹, imperfections on the surface of the microdisk cause backscattering that couples the initially degenerate traveling-wave WGMs. If the backscattering rate γ_β exceeds the total cavity loss rate κ_T , this mode-coupling results in the formation of standing wave modes which are split in frequency. The transmission scan of Fig. 2(a) illustrates this effect in our system, with $TE_{1,\pm 13}$ modes appearing as a resonance doublet with splitting $2\Delta\lambda_\beta = 31$ pm. Each mode has a linewidth of $\delta\lambda = 13$ pm, corresponding to $Q = 10^5$ and $\kappa_T/2\pi = 1.2$ GHz.

To tune the cavity into resonance with the X_a and X_b exciton lines of the QD we introduce nitrogen (N_2) gas into the cryostat^{22,27}. As described in Ref. [22] and in the Methods section, this allows for continuous and repeated tuning over a 4 nm wavelength range of the cavity modes. For the first set of measurements, we operate with an input power of 470 pW so that the system remains in a weak driving limit with the estimated bare-cavity intracavity photon number $n_{\text{cav}} = 0.03$. The normalized transmission and reflection spectra over a cavity tuning range of 240 pm are displayed as a two-dimensional intensity image in Fig. 2(b)-(c). Initially, we see a simple shift in the center wavelength of the cavity doublet mode, but once the cavity mode frequency nears the transition frequency of the higher-energy exciton line (X_a) of the QD, the spectra change dramatically. We see that coupling between the X_a -line and the cavity modes results in a significant spectral splitting (vacuum Rabi splitting) that is evidenced in the characteristic anti-crossing within both the transmitted and reflected signals. This anti-crossing is indicative of the cavity taking on the character of the QD exciton, and vice versa, when the system becomes strongly coupled. As the cavity is detuned red of the X_a -line, the spectra regain their initial bare-cavity doublet shape. Further tuning brings the cavity modes into resonance with the X_b exciton state. Only a small frequency shift of the cavity modes (no anti-crossing) is evident in this case, indicating that the X_b state only weakly couples to either cavity mode.

Figure 2(d) shows a series of reflection scans for a zoomed-in region of cavity tuning, near where the X_a -line and the cavity are in resonance. In general, the character of these spectra are complicated by the bimodal nature of WGM cavities. To adequately model the system, we use a quantum master equation (QME) as presented in Ref. [28]. The model is used to solve for the steady-state reflected and transmitted signals from the cavity as a function of parameters such as cavity-exciton cou-

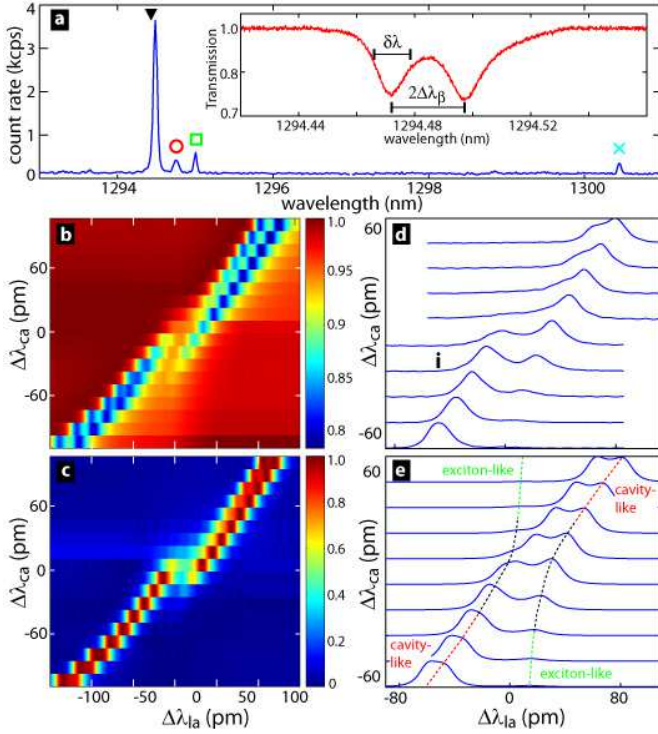


FIG. 2: **Reflection and transmission spectra from a strongly coupled microdisk-QD system.** **a**, Fiber-collected PL spectrum at a pump power of 30 nW showing the cavity mode (\blacktriangledown), X_a (\circ), X_b (\square), and X^- (\times) lines. The inset shows a transmission scan of the bare-cavity mode. **b**, Measured transmission and **c**, reflection spectra as a function of laser-QD detuning ($\Delta\lambda_{la}$) and cavity-QD detuning ($\Delta\lambda_{ca}$), where the cavity wavelength is tuned by the N_2 adsorption. Transmission and reflection spectra are normalized to unity. **d**, Experimental data and **e**, model plots for a series of reflected spectra in the central 120 pm region of cavity tuning. The dashed lines in **e** are guides-to-the-eye for the exciton-like and cavity-like tuning.

pling and excitonic dephasing (the bare-cavity properties are known from detuned cavity spectra). One other important parameter is the relative phase, ξ , between the surface-scattering and exciton mode coupling. The QD-cavity coupling strength with the standing wave modes, $g_{sw1,2}$, is modified relative to that for traveling wave WGMs by a factor of $(1 \pm e^{i\xi})/\sqrt{2}$.

A series of reflected spectra produced by the model is shown in Fig. 2(e) for a set of parameters, listed in Table I, which best estimates the measured reflected signal intensity, exciton linewidth, relative coupling to the two standing wave modes, and anti-crossed splitting. These parameters place the X_a exciton state and the $TE_{1,13}$ WGM in the good-cavity limit ($g > \gamma_{\perp} > \kappa_T$) of the strong coupling regime. We note that the achieved g_{sw1} is about six times smaller than the maximum possible value based on the cavity mode volume, and is likely due to the QD position being sub-optimal. We estimate that the QD is located 300-400-nm inwards from the position of peak field strength of the $TE_{1,13}$ mode (see Fig. 1(d)), with the dipole-moment of the X_a -line oriented radially and that of the X_b -line oriented azimuthally. This picture is

consistent with the orthogonal X_a - X_b polarization²⁶ and their relative measured coupling strengths.

The rate at which a single exciton can scatter incoming cavity photons is limited, resulting in a saturation in the strongly-coupled QD-cavity response for large enough input power. Two parameters used to characterize nonlinear processes in cQED are the critical atom number N_0 and saturation photon number m_0 , which gauge the number of atoms needed to alter the cavity response and the number of photons needed to saturate the atomic transition, respectively¹. These parameters are given by $N_0 = 2\kappa_T\gamma_{\perp}/g^2$ and $m_0 = \gamma_{\parallel}\gamma_{\perp}/4g^2$. In our system $N_0 = 0.44$ and $m_0 = 0.02$ for the standing wave mode (sw1) that couples most strongly to the QD. This indicates that a single QD strongly affects the cavity response (which Fig. 2 clearly indicates), while even an average intracavity photon number that is less than one can saturate the QD response.

The measured power dependence of the QD-cavity system is shown in Fig. 3, where the cavity is tuned into resonance with the X_a -line near the center of the anti-crossing region (scan marked 'i' in Fig. 2(d)), at which point the resonance peaks are nearly equal mixtures of exciton and cavity mode. Fig. 3(a) shows a plot of the measured reflected signal normalized to input power (ΔR) along with the modeled steady-state response of the cavity under weak driving conditions ($n_{cav} = 0.03$). As the input power to the cavity increases, Fig. 3(b) shows that the spectral splitting due to cavity-QD interaction ($2\Delta\lambda_g$) begins to diminish as the exciton saturates, and finally reaches a regime where the splitting is nearly two times smaller and due to surface-scattering ($2\Delta\lambda_{\beta}$). Fig. 3(c) plots the resulting mode splitting ($2\Delta\lambda_{g/\beta}$) and peak ΔR as a function of the optical drive power. Both the splitting and reflected signal begin to saturate towards their bare-cavity values for $n_{cav} = 0.1$. The QME model (dotted lines) predicts very similar behavior, albeit with a slightly higher drive power saturation point. Both data and model, however, show an extended saturation regime as expected due to the quantum fluctuations of a single dipole²⁹. Such saturation behavior has previously been experimentally observed in atomic systems³.

Use of an optical-fiber-based waveguide to efficiently probe the microcavity-QD system opens up many interesting possibilities for future devices and studies. In particular, excitation and collection through the optical channel allows for high resolution spectral and temporal studies of individual QD dynamics and a direct probe of the intra-cavity field. Studies of the quantum fluctuations of the strongly-coupled system¹⁷, through field and intensity correlations of the optical signal, are also now possible. An immediate application is the creation of an efficient fiber-coupled single photon source, while from a long-term perspective, it can be envisioned that the fiber interface can serve as a means to transfer quantum information to and from the QD. In comparison, atomic systems have the considerable advantages of homogeneity, much lower dephasing, and an energy level structure compatible with more complex manipulations of the quantum system. Nitrogen-vacancy centers in diamond^{9,30} have been viewed as a system that can provide some of the beneficial aspects of cold atoms. The measurement apparatus described here is equally applicable to this and other systems, and we are hopeful that it can be built upon

TABLE I: **Quantum master equation model parameters.** See Methods for definition of V_{tw} and η .

Parameter	V_{tw} $((\lambda/n)^3)$	η	$\kappa_e/2\pi$ (GHz)	$\kappa_i/2\pi$ (GHz)	$\gamma_\beta/2\pi$ (GHz)	ξ (rad.)	τ_{rad} (ns)	g_{sw1} (GHz)	g_{sw2} (GHz)	$\gamma_\perp/2\pi$ (GHz)	$\gamma_\parallel/2\pi$ (GHz)
Value	6.4	0.21	0.171	0.91	1.99	0.25π	1	2.93	1.21	1.17	0.55

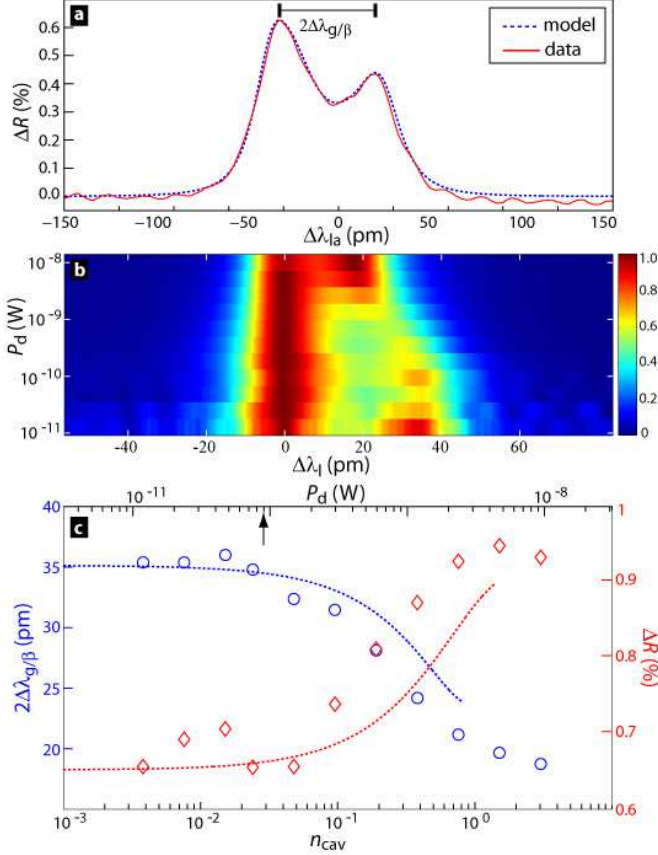


FIG. 3: **Power dependence of the QD-microcavity system.** **a**, Reflection spectrum from the QD-microdisk system near resonance (position (i) in Fig. 2) under weak driving. The solid red line is the measured reflected power normalized to input power; the dashed blue line is a QME model of the system. **b**, Normalized (to unity) reflected signal of panel a as a function of drive strength (dropped power in the bare-cavity, P_d) and detuning from the short-wavelength resonance peak ($\Delta\lambda_l$). **c**, Measured and modeled saturation of the mode splitting and peak reflected signal level versus drive strength (n_{cav} (bottom axis), P_d (top axis)). The model is only plotted up to a drive power of $n_{\text{cav}} = 1$ due to size limitations on the cavity mode Fock space which can be simulated.

to further progress the development of solid-state cQED nodes with microchip-scalability.

Methods

Device identification A linear array of microdisk cavities is fabricated, with the disk diameter of $2.5\mu\text{m}$ nominally held fixed. Fluctuations in lithog-

raphy cause the $\text{TE}_{1,13}$ mode wavelength to vary over a 1290-1310 nm range. We pump each device through the fiber taper and on resonance with one of its WGMs in the 980 nm band²⁴. This selectively excites QDs that lie in the disk periphery and overlap with the $\text{TE}_{1,13}$ mode. For those devices in which isolated QD emission is observed, we examine the spectral position of the $\text{TE}_{1,13}$ mode relative to the QD states through PL and cavity transmission. A digital wet etching process²⁵ provides a cavity mode blue shift of 0.8 nm/cycle. This wet etch is repeated until the cavity mode lies blue (and within 1 nm) of the desired QD single exciton lines. N_2 adsorption is then used to red-shift the mode into resonance with the desired exciton line.

Transmission/Reflection measurements The tunable laser used in transmission measurements provides a narrowband single mode laser line (< 5 MHz) and continuous wavelength tuning through dithering of a piezo element. The transmitted and reflected signals are detected by TE-cooled (1 kHz bandwidth) and LN_2 -cooled (150 Hz bandwidth) InGaAs photodetectors, respectively. In order to reduce detector noise the transmission and reflection signals are low-pass filtered (30 Hz cut-off) and the scans are averaged 10-20 times to produce the spectra of Fig. 2. PL is spectrally dispersed through a 550 mm Czerny-Turner spectrometer and detected on a 512 element LN -cooled InGaAs array ($25\mu\text{m} \times 500\mu\text{m}$ pixel size). The effective spectrometer resolution is 35 pm.

Cavity tuning Nitrogen is released into the chamber in discrete 5 second increments, with the flow rate adjusted so that a tuning level of ~ 10 pm/step is achieved. Once the shift is complete, the transmission and reflection spectra are acquired as described above. At temperatures above 28 K, the N_2 can be removed from the disk surface and the cavity mode reset back to its original wavelength allowing for repeated tuning cycles.

Effective mode volume and g The FEM-calculated traveling wave mode volume of the $\text{TE}_{1,13}$ WGM is $V_{\text{tw}} = 6.4(\lambda/n)^3$. The coherent coupling rate of the exciton to the traveling wave mode is $g_{\text{tw}} = \eta\sqrt{3c\lambda_0^2/8\pi n^3\tau_{\text{sp}}V_{\text{tw}}}$, where η accounts for the position and orientation of the exciton dipole ($\eta = 1$ for an exciton dipole oriented parallel with, and positioned at, the peak of the cavity mode electric field).

Quantum master equation simulations Reference [28] presents an appropriate model for our system. We numerically solve the steady-state QME for the system's density matrix, from which the transmitted and reflected spectra from the cavity are generated. A Fock space dimension of 6 for each cavity mode was used in modeling the drive power dependence of the system shown in Fig. 3. The expectation of the commutation between creation and annihilation operators for each mode was calculated to ensure accuracy of the simulation.

Acknowledgements

The authors thank Sanjay Krishna and Andreas Stintz of the Center for High Technology Materials at the University of New Mexico for providing material growth in support of this work.

-
- ¹ H. J. Kimble, *Physica Scripta* **T76**, 127 (1998).
 - ² H. Mabuchi and A. C. Doherty, *Science* **298**, 1372 (2002).
 - ³ C. J. Hood, M. S. Chapman, T. W. Lynn, and H. J. Kimble, *Phys. Rev. Lett.* **80**, 4157 (1998).
 - ⁴ M. Hennrich, T. Legero, A. Kuhn, and G. Rempe, *Phys. Rev. Lett.* **85**, 4872 (2000).
 - ⁵ A. Boca, R. Miller, K. M. Birnbaum, A. D. Boozer, J. McKeever, and H. J. Kimble, *Phys. Rev. Lett.* **93**, 233603 (2004).
 - ⁶ M. Keller, B. Lange, K. Hayaska, W. Lange, and H. Walther, *Nature* **431**, 1075 (2004).
 - ⁷ T. Aoki, B. Dayan, E. Wilcut, W. P. Bowen, A. S. Parkins, H. J. Kimble, T. J. Kippenberg, and K. J. Vahala, *Nature* **443**, 671 (2006).
 - ⁸ Y. Colombe, T. Steinmetz, G. Dubois, F. Linke, D. Hunger, and J. Reichel (2007), [quant-ph/0706.1390](https://arxiv.org/abs/quant-ph/0706.1390).
 - ⁹ Y.-S. Park, A. K. Cook, and H. Wang, *Nano Letters* **6**, 2075 (2006).
 - ¹⁰ J. P. Reithmaier, G. Sek, A. Loffer, C. Hoffman, S. Kuhn, S. Reitzenstein, L. V. Keldysh, V. D. Kulakovskii, T. L. Reinecke, and A. Forchel, *Nature* **432**, 197 (2004).
 - ¹¹ T. Yoshie, A. Scherer, J. Hendrickson, G. Khitrova, H. Gibbs, G. Rupper, C. Ell, Q. Schenkin, and D. Deppe, *Nature* **432**, 200 (2004).
 - ¹² E. Peter, P. Senellart, D. Martrou, A. Lemaître, J. Hours, J. M. Gérard, and J. Bloch, *Phys. Rev. Lett.* **95**, 067401 (2005).
 - ¹³ K. Hennessy, A. Badolato, M. Winger, D. Gerace, M. Atature, S. Guide, S. Falt, E. Hu, and A. Imamoglu, *Nature (London)* **445**, 896 (2007).
 - ¹⁴ D. Press, S. Gotzinger, S. Reitzenstein, C. Hoffmann, A. Löffler, M. Kamp, A. Forchel, and Y. Yamamoto, *Phys. Rev. Lett.* **98**, 117402 (2007).
 - ¹⁵ P. Michler, A. Kiraz, C. Becher, W. V. Schoenfeld, P. M. Petroff, L. Zhang, E. Hu, and A. Imamoglu, *Science* **290**, 2282 (2000).
 - ¹⁶ C. Santori, D. Fattal, J. Vuckovic, G. Solomon, and Y. Yamamoto, *Nature* **419**, 594 (2002).
 - ¹⁷ K. M. Birnbaum, A. Boca, R. Miller, A. Boozer, T. E. Northup, and H. J. Kimble, *Nature* **436**, 87 (2005).
 - ¹⁸ J. C. Knight, G. Cheung, F. Jacques, and T. A. Birks, *Opt. Lett.* **22**, 1129 (1997).
 - ¹⁹ S. M. Spillane, T. J. Kippenberg, O. J. Painter, and K. J. Vahala, *Phys. Rev. Lett.* **91**, 043902 (2003).
 - ²⁰ K. Srinivasan, P. E. Barclay, M. Borselli, and O. Painter, *Phys. Rev. B* **70**, 081306R (2004).
 - ²¹ K. Srinivasan, M. Borselli, T. J. Johnson, P. E. Barclay, O. Painter, A. Stintz, and S. Krishna, *Appl. Phys. Lett.* **86**, 151106 (2005).
 - ²² K. Srinivasan and O. Painter, *Appl. Phys. Lett.* **90**, 031114 (2007).
 - ²³ G. T. Liu, A. Stintz, H. Li, T. C. Newell, A. L. Gray, P. M. Varangis, K. J. Malloy, and L. F. Lester, *IEEE J. Quan. Elec.* **36**, 1272 (2000).
 - ²⁴ K. Srinivasan, O. Painter, A. Stintz, and S. Krishna (2007), [physics/0706.1831](https://arxiv.org/abs/physics/0706.1831).
 - ²⁵ A. Badolato, K. Hennessy, M. Atature, J. Dreiser, E. Hu, P. M. Petroff, and A. Imamoglu, *Science* **308**, 1158 (2005).
 - ²⁶ V. D. Kulakovski, G. Bacher, , R. Weigand, T. Kummell, A. Forchel, E. Borovitskaya, K. Leonardi, and D. Hommel, *Phys. Rev. Lett.* **82**, 1780 (1999).
 - ²⁷ S. Mosor, J. Hendrickson, B. C. Richards, J. Sweet, G. Khitrova, H. Gibbs, T. Yoshie, A. Scherer, O. B. Shchekin, and D. G. Deppe, *Appl. Phys. Lett.* **87**, 141105 (2005).
 - ²⁸ K. Srinivasan and O. Painter, *Phys. Rev. A* **75**, 023814 (2007).
 - ²⁹ C. M. Savage and H. J. Carmichael, *IEEE J. Quan. Elec.* **24**, 1495 (1988).
 - ³⁰ C. Santori, P. Tamarat, P. Neumann, J. Wrachtrup, D. Fattal, R. Beausoleil, J. Rabeau, P. Olivero, A. Greentree, S. Prawer, et al., *Phys. Rev. Lett.* **97**, 247401 (2006).